

## Article

# Facile Synthesis and Characterization of Novel Nanostructures for the Efficient Disposal of Crystal Violet Dye from Aqueous Media

Ehab A. Abdelrahman <sup>1,2,\*</sup> , Faisal K. Algethami <sup>1</sup> , Huda S. AlSalem <sup>3</sup> , Mona S. Binkadem <sup>4</sup> ,  
Fawaz A. Saad <sup>5</sup>, Gharieb S. El-Sayyad <sup>6,7</sup>, Nadeem Raza <sup>1,8</sup> and Khalil ur Rehman <sup>9</sup>

- <sup>1</sup> Department of Chemistry, College of Science, Imam Mohammad Ibn Saud Islamic University (IMSIU), Riyadh 11623, Saudi Arabia; falgethami@imamu.edu.sa (F.K.A.); nrmostafa@imamu.edu.sa (N.R.)
  - <sup>2</sup> Chemistry Department, Faculty of Science, Benha University, Benha 13518, Egypt
  - <sup>3</sup> Department of Chemistry, College of Science, Princess Nourah bint Abdulrahman University, P.O. Box 84428, Riyadh 11671, Saudi Arabia; husalsalem@pnu.edu.sa
  - <sup>4</sup> Department of Chemistry, College of Science, University of Jeddah, P.O. Box 80327, Jeddah 21589, Saudi Arabia; 04100507@uj.edu.sa
  - <sup>5</sup> Department of Chemistry, Faculty of Applied Sciences, Umm Al-Qura University, Makkah 21955, Saudi Arabia; fasaad@uqu.edu.sa
  - <sup>6</sup> Microbiology and Immunology Department, Faculty of Pharmacy, Ahram Canadian University (ACU), Giza 12451, Egypt; gharieb.elsayyad@gu.edu.eg
  - <sup>7</sup> Microbiology and Immunology Department, Faculty of Pharmacy, Galala University, Galala City, Suez 11566, Egypt
  - <sup>8</sup> Department of Chemistry, Govt. Alamdar Hussain Islamia Degree College, Multan, Pakistan
  - <sup>9</sup> Institute of Chemical Sciences, Gomal University, Dera Ismail Khan, KPK, Pakistan; rehmakhalil025@gmail.com
- \* Correspondence: eaaahmed@imamu.edu.sa or dr.ehabsaleh@yahoo.com



**Citation:** Abdelrahman, E.A.; Algethami, F.K.; AlSalem, H.S.; Binkadem, M.S.; Saad, F.A.; El-Sayyad, G.S.; Raza, N.; Rehman, K.u. Facile Synthesis and Characterization of Novel Nanostructures for the Efficient Disposal of Crystal Violet Dye from Aqueous Media. *Inorganics* **2023**, *11*, 339. <https://doi.org/10.3390/inorganics11080339>

Academic Editors: Carlos Martínez-Boubeta and Eleonora Aneggi

Received: 30 June 2023

Revised: 8 August 2023

Accepted: 14 August 2023

Published: 17 August 2023



**Copyright:** © 2023 by the authors. Licensee MDPI, Basel, Switzerland. This article is an open access article distributed under the terms and conditions of the Creative Commons Attribution (CC BY) license (<https://creativecommons.org/licenses/by/4.0/>).

**Abstract:** An excessive accumulation of crystal violet dye in the human body results in an accelerated heart rate, tetraplegia, eye irritation, and long-term damage to the transparent mucous membrane that protects the eyeballs. Accordingly, in this paper, sodium manganese silicate/sodium manganese silicate hydroxide hydrate was easily fabricated as a novel type of nanostructures for the successful disposal of crystal violet dye from aqueous solutions. The formed sodium manganese silicate/sodium manganese silicate hydroxide hydrate nanostructures after the hydrothermal treatment of the gel produced from the interaction of Mn(II) ions with Si(IV) ions at 180 °C for 6, 12, 18, and 24 h were abbreviated as MS1, MS2, MS3, and MS4, respectively. The XRD showed that the average crystallite size of the MS1, MS2, MS3, and MS4 samples is 8.38, 7.43, 4.25, and 8.76 nm, respectively. The BET surface area of the MS1, MS2, MS3, and MS4 samples is 41.58, 46.15, 58.25, and 39.69 m<sup>2</sup>/g, respectively. The MS1, MS2, MS3, and MS4 samples consist of spherical and irregular shapes with average grain sizes of 157.22, 88.06, 43.75, and 107.08 nm, respectively. The best adsorption conditions of the crystal violet dye employing the MS1, MS2, MS3, and MS4 products were achieved at pH = 8, contact time = 140 min, and solution temperature = 298 kelvin. The linear pseudo-2nd-order model as well as the linear Langmuir isotherm better describe the disposal of the crystal violet dye using the MS1, MS2, MS3, and MS4 adsorbents. The studied thermodynamic parameters indicated that the disposal of the crystal violet dye employing the MS1, MS2, MS3, and MS4 adsorbents is spontaneous, exothermic, and chemical. The maximum disposal capacities of the MS1, MS2, MS3, and MS4 adsorbents towards crystal violet dye are 342.47, 362.32, 411.52, and 310.56 mg/g, respectively.

**Keywords:** nanoadsorbents; adsorption; water treatment; crystal violet dye

## 1. Introduction

The expansion of the science, industrial, and technology sectors improves the quality of human life. It had a similar effect to the increased environmental pollution caused by the

release of pollutants into water bodies [1–4]. Contaminated water is without a doubt one of the most attention-grabbing issues that influences the environment, humans, wildlife, and aquatic flora. Dangerous constituents causing water contamination include medicinal components, organic dyes, industrial chemicals, and agricultural effluents [5–9]. Due to their antagonistic and harmful influences on the environment, dyes have attracted special attention in wastewater treatment [10–14]. The dyes have made significant contributions to the improvement of human life in the fields of paints, leather industries, fabrics, food processing industries, etc. On the other hand, the pollutants from these industries have a severe impact on the environment and are therefore hazardous to humans and other species. Due to their toxicity, carcinogenicity, and mutagenicity, organic dyes have become the leading cause of water contamination [15,16]. Crystal violet is a widely used organic cationic dye belonging to the triphenylmethane family. It is used extensively in leather processing, commercial fabric dyeing, biological stains, veterinary medicines, and the food industry [17–19]. Increased heart rate, tetraplegia, eye irritation, and long-term damage to the transparent mucous membrane protecting the eyeballs are caused by an excessive accumulation of crystal violet dye in the human body [20]. Consequently, the removal of crystal violet dye from toxic wastewater is important. Various techniques for the decontamination of crystal violet dye have been described in the literature. These include electrolysis, biological treatment, flocculation, membrane filtration, adsorption, advanced oxidation, and photocatalytic degradation [21–24]. Among these, the adsorption method has been regarded as a flexible procedure for wastewater management. It offers significant advantages, including affordability, low cost, profitability, performance, and service simplicity, compared to other conventional techniques [25–30]. There are a lot of adsorbents for the removal of crystal violet dye such as natural zeolite (177.75 mg/g), activated carbon/chitosan composite (2.38 mg/g), pyrophyllite (9.58 mg/g),  $\text{Fe}_3\text{O}_4$ /sodium dodecyl sulphate (166.70 mg/g), multi-walled carbon nanotubes (90.52 mg/g), aromatic polyimides (303.03 mg/g), polyacrylonitrile (5.46 mg/g), and activated carbon/ $\text{Fe}_3\text{O}_4$  composite (35.30 mg/g) [20,31–37]. However, there is a need for more effective adsorbents. Recently, manganese-based materials have important uses in several fields such as supercapacitors and water treatment [38,39]. Consequently, the principal objective of this work was to hydrothermally synthesize sodium manganese silicate/sodium manganese silicate hydroxide hydrate as novel nanostructures for the effective disposal of crystal violet dye from the aqueous solutions. In the crystal lattice of nanostructures, some of Mn(II) ions replace some Si(IV) ions, creating a negative charge that is chemically neutralized by the Na(I) ions, which have the ability to do ion exchange with positive ions such as crystal violet dye. Other objectives of this work included the study of experimental effects on the disposal of crystal violet dye, such as pH, contact time, initial concentration of crystal violet dye, and temperature. Also, the synthesized nanostructures were characterized using several tools such as X-ray diffraction (XRD), Energy dispersive X-ray (EDX), Fourier-transform infrared spectroscopy (FT-IR), and scanning electron microscopy (SEM).

## 2. Experimental

### 2.1. Chemicals

Hydrochloric acid (HCl), Manganese acetate tetrahydrate ( $\text{Mn}(\text{CH}_3\text{COO})_2 \cdot 4\text{H}_2\text{O}$ ), sodium metasilicate pentahydrate ( $\text{Na}_2\text{SiO}_3 \cdot 5\text{H}_2\text{O}$ ), crystal violet dye ( $\text{C}_{25}\text{H}_{30}\text{ClN}_3$ ), and sodium hydroxide (NaOH) were supplied from Sigma Aldrich Company and utilized without additional chemical refining.

### 2.2. Synthesis of Sodium Manganese Silicate/Sodium Manganese Silicate Hydroxide Hydrate

The Si(IV) solution was freshly prepared by dissolving 15 g of  $\text{Na}_2\text{SiO}_3 \cdot 5\text{H}_2\text{O}$  in 60 mL of bi-distilled water. In addition, the Mn(II) solution was freshly prepared via dissolving 4.42 g of  $\text{Mn}(\text{CH}_3\text{COO})_2 \cdot 4\text{H}_2\text{O}$  in 60 mL of bi-distilled water. After that, the Mn(II) solution was carefully added using a burette to the Si(IV) solution drop by drop with vigorous stirring for 30 min. Additionally, the yielded gel was carefully charged into a 180 mL

Teflon-lined stainless-steel autoclave then treated hydrothermally at 180 °C for 6, 12, 18, and 24 h. Moreover, the formed sodium manganese silicate/sodium manganese silicate hydroxide hydrate nanostructures after 6, 12, 18, and 24 h were filtered using a centrifuge, washed several times with hot bi-distilled water, oven dried at 65 °C, and encoded as MS1, MS2, MS3, and MS4, respectively.

### 2.3. Characterization

Using an X-ray diffraction (XRD) apparatus (Model: Bruker D8 Advance (Billerica, MA, USA)), the chemical structures of the MS1, MS2, MS3, and MS4 nanostructures were examined. Operating a Fourier transform infrared (FT-IR) instrument (Model: Nicolet iS50 (Waltham, MA, USA)), the chemical functional groups of the MS1, MS2, MS3, and MS4 samples were recognized. The surface morphology and chemical elements of the MS1, MS2, MS3, and MS4 products were precisely recognized by scanning electron microscopy (Model: SEM-JEOL 6510LA (Akishima, Japan)) coupled to an energy-dispersive X-ray (EDX) unit. Furthermore, the surface properties of the MS1, MS2, MS3, and MS4 products were investigated operating N<sub>2</sub> adsorption/desorption analysis at −196 °C on a Quantachrome instrument (Model: NOVA Touch LX2 (Kiev, Ukraine)). Using a Jasco V-670 ultraviolet-visible spectrometer (Hachioji-shi, Japan), the concentration change of the crystal violet dye was measured.

### 2.4. Disposal of Crystal Violet Dye from Aqueous Media

The adsorption of crystal violet dye was conducted using a batch experiment. In this regard, 0.05 g of the MS1, MS2, MS3, or MS4 adsorbent was carefully added to about 100 mL of a 250 mg/L crystal violet dye solution. After that, the mixture was magnetically stirred for the specified time then the adsorbent was removed by centrifugation technique. At a maximum absorbance wavelength of 590 nm, the concentration of crystal violet dye in the filtrate was determined using a Jasco V-670 ultraviolet-visible spectrophotometer. The effect of pH on crystal violet dye removal at room temperature was accomplished in the range from 2 to 8, where the contact time equals 3 h. The pH was adapted using 0.1 M NaOH and HCl. The effect of contact time on crystal violet dye removal at room temperature was accurately accomplished in the range from 20 min to 180 min, where the pH equals 8. The effect of temperature on crystal violet dye removal after 140 min was accurately accomplished in the range from 298 kelvin to 180 kelvin, where the pH equals 8. The effect of concentration on crystal violet dye removal after 140 min was accomplished in the range from 150 mg/L to 300 mg/L, where the pH equals 8.

The disposal percentage (%R) of crystal violet dye utilizing the MS1, MS2, MS3, and MS4 adsorbents was expressed using Equation (1) [40].

$$\% R = \frac{C_o - C_e}{C_o} \times 100 \quad (1)$$

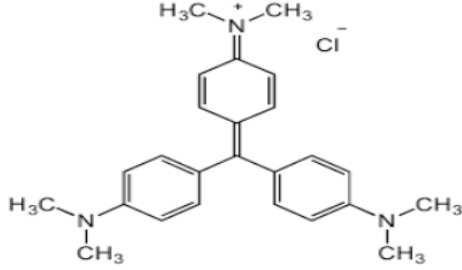
where,  $C_o$  is the initial concentration of crystal violet dye (mg/L) and  $C_e$  is the equilibrium concentration of crystal violet dye (mg/L).

The disposal capability ( $Q$ , mg/g) of the MS1, MS2, MS3, and MS4 adsorbents towards crystal violet dye was expressed using Equation (2) [40].

$$Q = (C_o - C_e) \times \frac{V}{W} \quad (2)$$

where,  $W$  is the weight of the MS1, MS2, MS3, and MS4 adsorbents (g).  $V$  is the solution volume of the crystal violet dye (L). The characteristics of crystal violet dye are clarified in Table 1.

**Table 1.** Characteristics of crystal violet dye.

Structure formula	
Chemical formula	C <sub>25</sub> H <sub>30</sub> ClN <sub>3</sub>
Molar mass	407.99 g/mol
Solubility	Soluble in water
Maximum Wavelength	590 nm

The point of zero charge ( $\text{pH}_{\text{PZC}}$ ) of the MS1, MS2, MS3, and MS4 adsorbents was determined following the procedure outlined by Khalifa et al. [40]. The method involved the addition of 0.20 g of each adsorbent to separate 50 mL solutions of 0.02 M KCl. The initial pH ( $\text{pH}_{\text{initial}}$ ) of the KCl solutions ranged from 2.5 to 11.5. After stirring each mixture of KCl and adsorbent for 5 h, the subsequent pH values ( $\text{pH}_{\text{final}}$ ) were measured and plotted against the corresponding primary pH values ( $\text{pH}_{\text{initial}}$ ). The pH at which a distinct plateau was observed in the plot was identified as the  $\text{pH}_{\text{PZC}}$ .

### 3. Results and Discussion

#### 3.1. Discussion of Characterization of the Synthesized Samples

Figure 1A–D represents the XRD patterns of the MS1, MS2, MS3, and MS4 samples, respectively. All the samples consist of sodium manganese silicate ( $\text{Na}_5(\text{Mn}_{0.67}\text{Na}_{0.33})_3\text{MnSi}_6\text{O}_{18}$ ) and sodium manganese silicate hydroxide hydrate ( $\text{Na}_4\text{Mn}_5\text{Si}_{10}\text{O}_{24}(\text{OH})_6 \cdot 6\text{H}_2\text{O}$ ) as indicated by JCPDS Nos. 01-072-2251 and 00-039-0405, respectively. The peaks of the sodium manganese silicate at  $2\theta = 21.79^\circ$ ,  $25.15^\circ$ ,  $56.67^\circ$ , and  $66.26^\circ$  are due to the (012), (120), (340), and (136) miller indices, respectively. Furthermore, the peaks of the sodium manganese silicate hydroxide hydrate at  $2\theta = 6.09^\circ$ ,  $12.44^\circ$ , and  $32.84^\circ$  are due to the (010), (112), and (143) miller indices, respectively. Additionally, the average crystallite size of the MS1, MS2, MS3, and MS4 samples is 8.38, 7.43, 4.25, and 8.76 nm, respectively. Hence, we can conclude that the MS1, MS2, MS3, and MS4 samples consist of the same phases (sodium manganese silicate and sodium manganese silicate hydroxide hydrate) but they differ in intensities of XRD peaks and hence they have different average crystallite sizes and surface textures. The consequent surface textures such as surface area, which will be discussed later. Hence, increasing the hydrothermal time from 6 h to 18 h reduces the average crystallite size of the products. Besides, increasing the hydrothermal time from 18 h to 24 h increases the average crystallite size of the synthesized products.

Figure 2A–D displays the EDX patterns of the MS1, MS2, MS3, and MS4 nanostructures, respectively. All the products consist of Mn, Si, Na, and O, as displayed in Table 2.

Figure 3A–D displays the adsorption/desorption curves of  $\text{N}_2$  on the MS1, MS2, MS3, and MS4 products, respectively. In addition, the obtained curves of all the synthesized nanostructures belong to the IV types [41]. Moreover, the surface properties, for example, total pore volume, BET surface area as well as average pore size of the MS1, MS2, MS3, and MS4 samples are displayed in Table 3. The determined BET surface area increased according to the following order;  $\text{MS4} < \text{MS1} < \text{MS2} < \text{MS3}$  because the average crystallite size improved according to the reverse sequence.

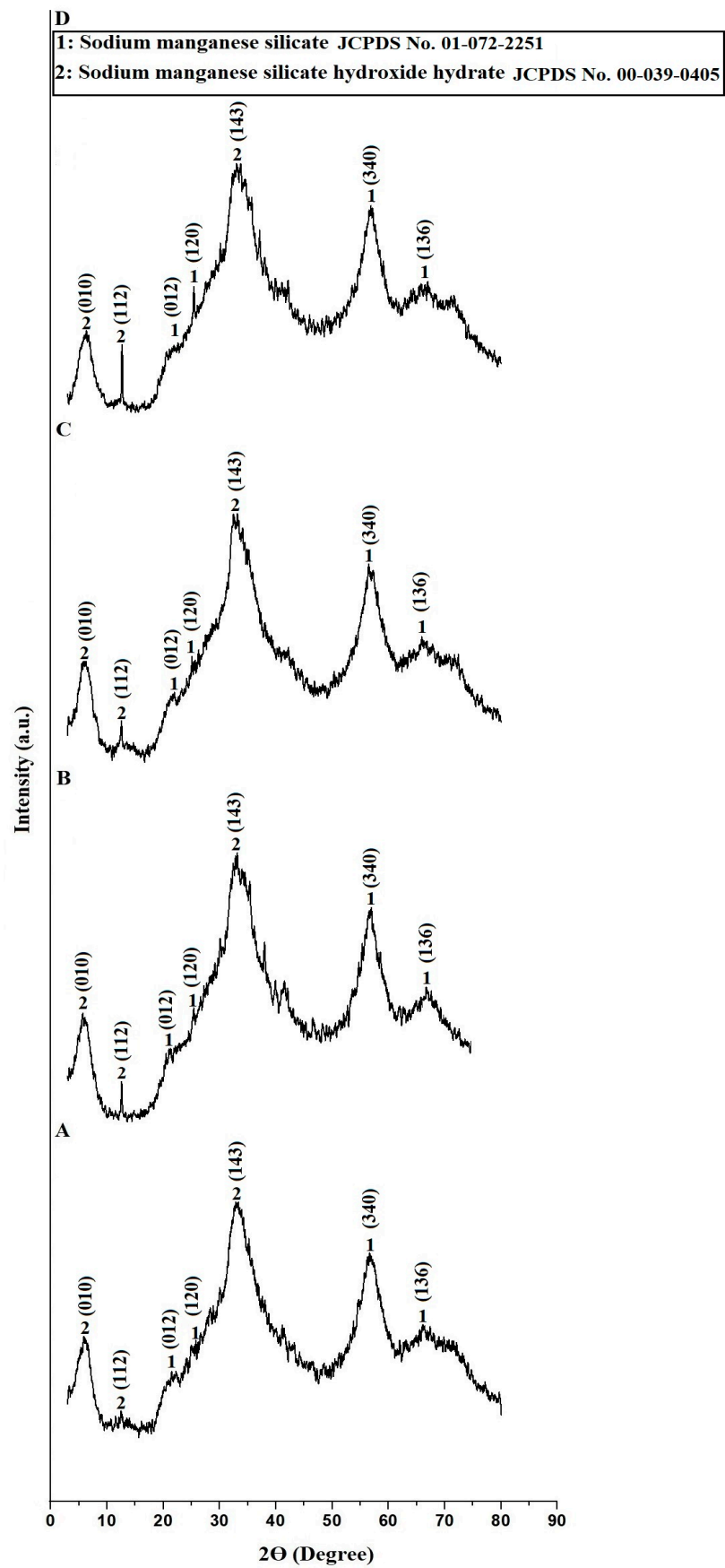
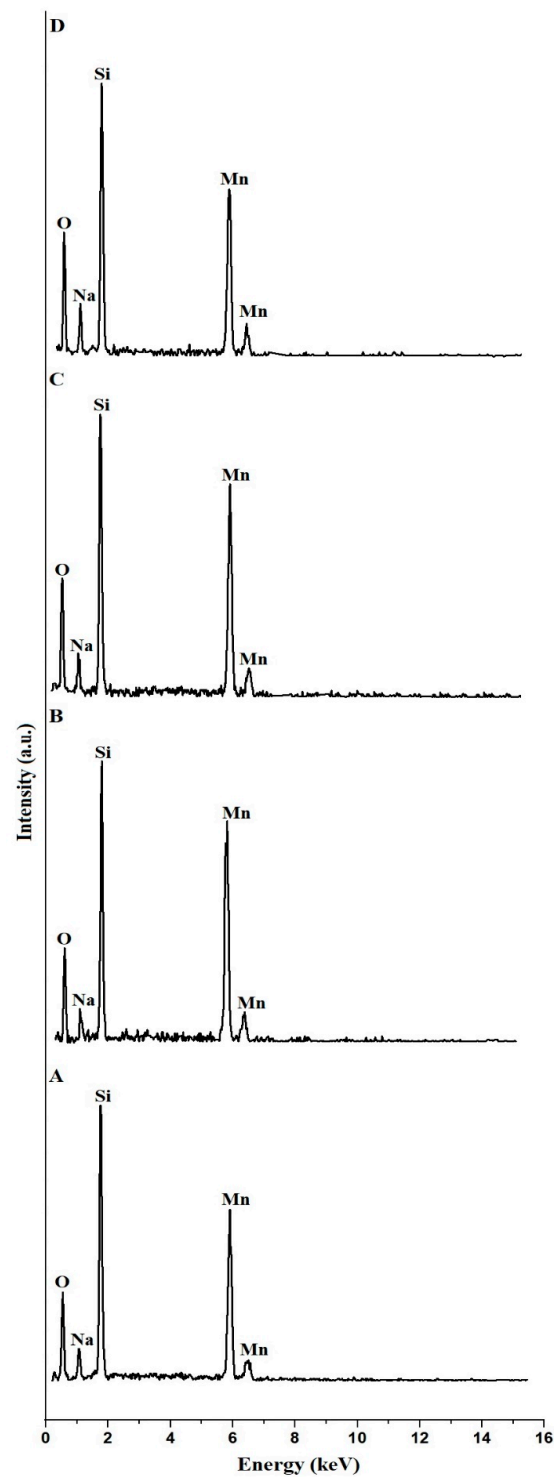


Figure 1. The XRD patterns of the MS1 (A), MS2 (B), MS3 (C), and MS4 (D) products.



**Figure 2.** The EDX patterns of the MS1 (A), MS2 (B), MS3 (C), and MS4 (D) samples.

**Table 2.** The EDX analysis of the MS1, MS2, MS3, and MS4 nanostructures.

Samples	% Mn	% Si	% Na	% O
MS1	28.97	32.04	9.20	29.79
MS2	35.03	30.44	8.08	26.45
MS3	31.07	28.26	11.53	29.14
MS4	27.17	28.06	11.95	32.82

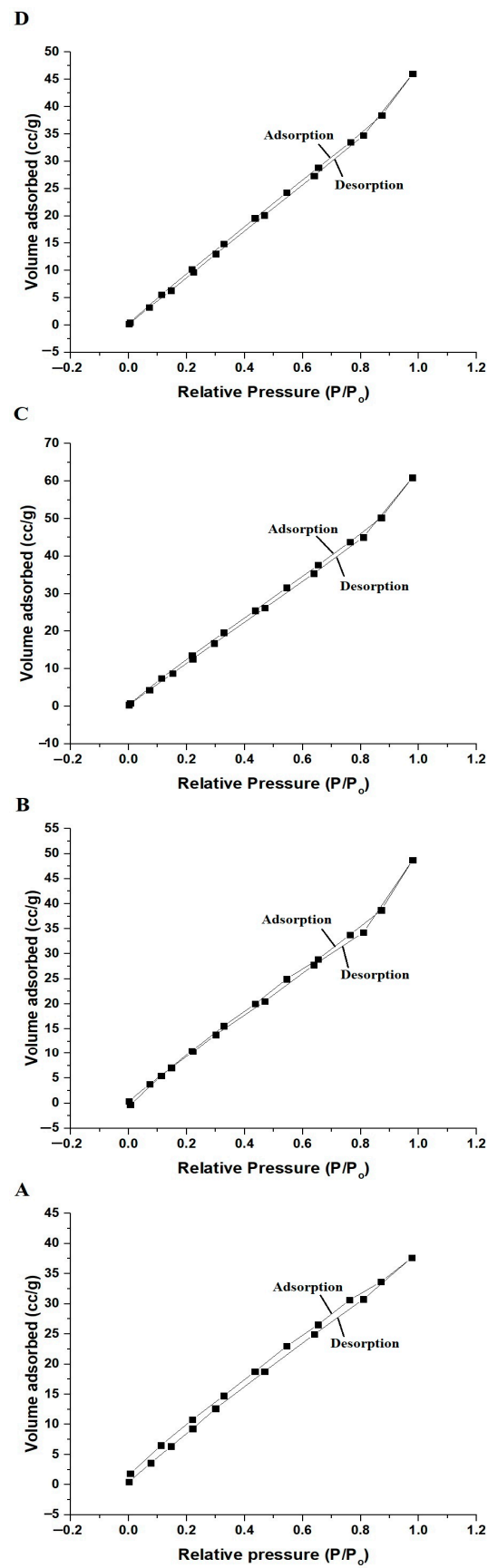


Figure 3. The  $N_2$  adsorption/desorption isotherms of the MS1 (A), MS2 (B), MS3 (C), and MS4 (D) samples.

**Table 3.** The obtained BET surface area, average pore size as well as total pore volume of the MS1, MS2, MS3, and MS4 products.

Surface Properties	Sample			
	MS1	MS2	MS3	MS4
BET surface area (m <sup>2</sup> /g)	41.58	46.15	58.25	39.69
Average pore size (nm)	2.81	3.27	3.24	3.09
Total pore volume (cc/g)	0.0584	0.0755	0.0945	0.0714

Figure 4A–D displays the SEM images of the MS1, MS2, MS3, and MS4 nanostructures, respectively. The MS1, MS2, MS3, and MS4 nanostructures consist of spherical and irregular shapes with average grain sizes of 157.22, 88.06, 43.75, and 107.08 nm, respectively. There is inconsistency between the average crystallite size and the grain size of the samples. X-ray diffraction (XRD) and scanning electron microscopy (SEM) are two different techniques used to characterize materials, and they provide information on different aspects of the sample microstructure, including crystallite size and grain size, respectively. The main difference between the crystallite size obtained from XRD and the grain size obtained from SEM is the level of structural information they provide. XRD gives information about the size of the individual crystalline domains within the material, while SEM provides information about the size and shape of the individual grains of surface that make up the material, which may include multiple crystalline domains.

Figure 5A–D displays the FT-IR spectra of the MS1, MS2, MS3, and MS4 nanostructures, respectively. In addition, the apparent absorption bands in the range 450–465 cm<sup>-1</sup> are related to the bending vibration of the E-O-E (E = Si and/or Mn). The apparent absorption bands in the range 610–668 cm<sup>-1</sup> are related to the internal symmetric stretching of the E-O-E (E = Si and/or Mn). The apparent absorption bands in the range 775–784 cm<sup>-1</sup> are related to the external symmetric stretching of the E-O-E (E = Si and/or Mn). The apparent absorption bands in the range 1006–1016 cm<sup>-1</sup> are related to the internal asymmetric stretching of the E-O-E (E = Si and/or Mn). The apparent absorption bands in the range 1413–1422 cm<sup>-1</sup> are related to the external asymmetric stretching of the E-O-E (E = Si and/or Mn). The apparent absorption bands in the range 1559–1655 cm<sup>-1</sup> are related to the bending vibration of the OH. The apparent absorption bands in the range 3446–3462 cm<sup>-1</sup> are related to the stretching vibration of the OH [41,42].

### 3.2. Disposal of Crystal Violet Dye from Aqueous Media

#### 3.2.1. Effect of Solution pH

The pH of the organic dye solution has a major impact on the adsorption mechanism and performance. The solution's pH has a direct influence on the surface charge of the adsorbent and the extent of ionization of the adsorbate molecules. Consequently, in the adsorption process involving the surface charge of the adsorbent, the pH of the organic dye solution will have a substantial effect on adsorption performance. This study investigated the adsorption performance of the MS1, MS2, MS3, and MS4 adsorbents for crystal violet dye removal at different pH values, ranging from 2 to 8, using an initial crystal violet dye concentration of 250 mg/L for 3 h at room temperature. The adsorption of crystal violet dye cannot be studied at pH greater than 8 due to the possibility of precipitation. Crystal violet dye is a cationic dye, meaning it carries a positive charge. As the pH increases above 8, the solution becomes more basic, and there is a higher concentration of hydroxide ions (OH<sup>-</sup>). These hydroxide ions can interact with the positively charged dye molecules, leading to charge neutralization and the formation of insoluble precipitates. The impact of initial pH on the % disposal of crystal violet dye and the disposal capability of the MS1, MS2, MS3, and MS4 adsorbents is depicted in Figure 6A,B, respectively. It is evident that the % disposal of crystal violet dye and the disposal capability of the MS1, MS2, MS3, and MS4 adsorbents were extremely sensitive to the initial pH of the crystal violet dye solution. The higher the pH value, the higher the resulting % disposal or disposal capability. This

result implies that the disposal process is primarily controlled by the electrostatic attraction between the surface of the utilized adsorbent and the adsorbate molecules. At pH = 8, the % disposal of the crystal violet dye using the MS1, MS2, MS3, and MS4 adsorbents is 67.96, 70.78, 81.89, and 61.87%, respectively. Besides, the maximum disposal capability of the MS1, MS2, MS3, and MS4 adsorbents towards crystal violet dye is 339.82, 353.92, 409.44, and 309.36 mg/g, respectively. The % disposal and disposal capability increased according to the following order; MS4 < MS1 < MS2 < MS3 because the obtained BET surface area increased in the same order.

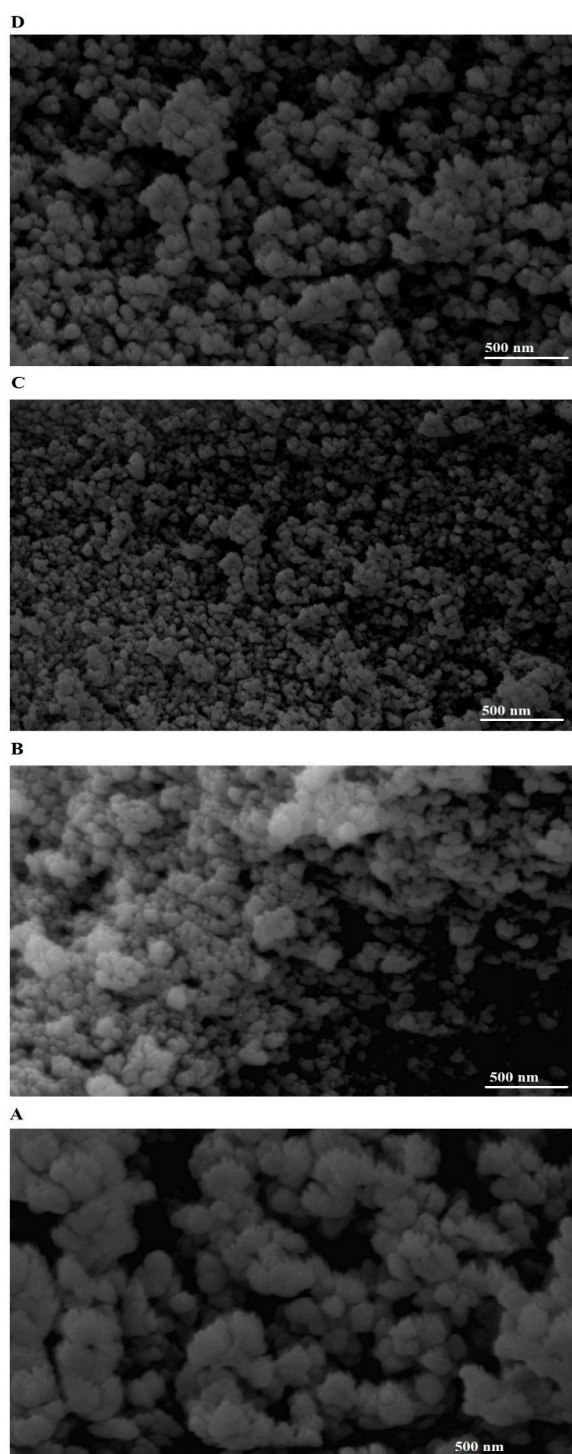


**Figure 4.** The SEM images of the MS1 (A), MS2 (B), MS3 (C), and MS4 (D) nanostructures.

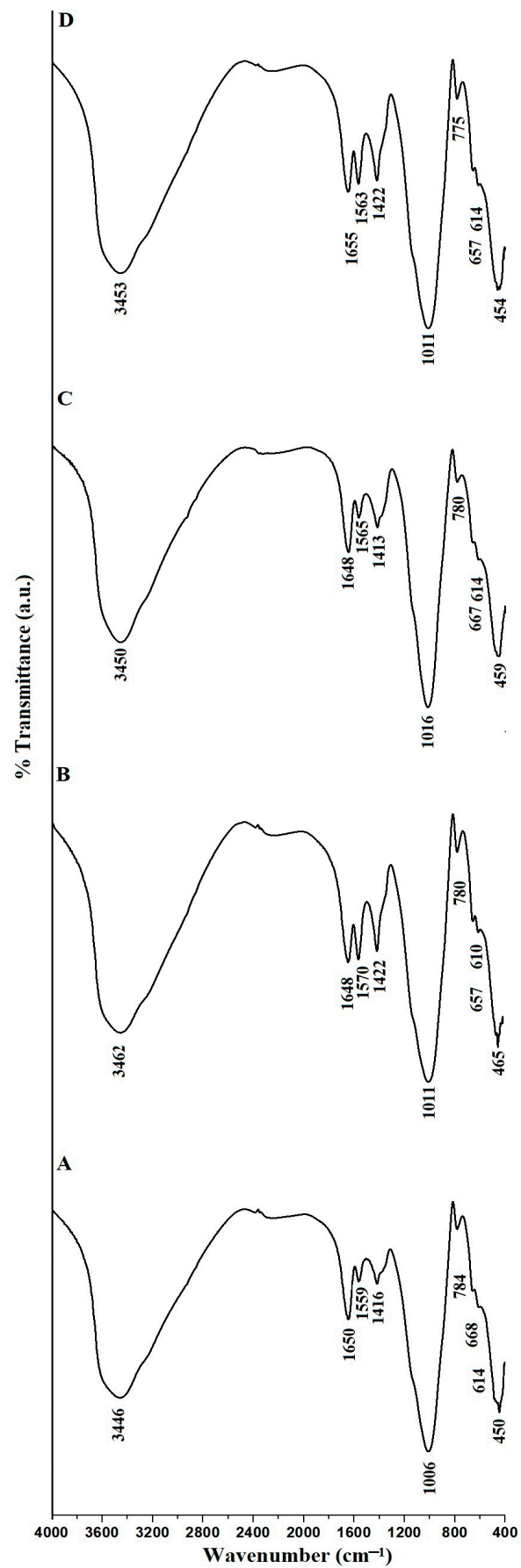
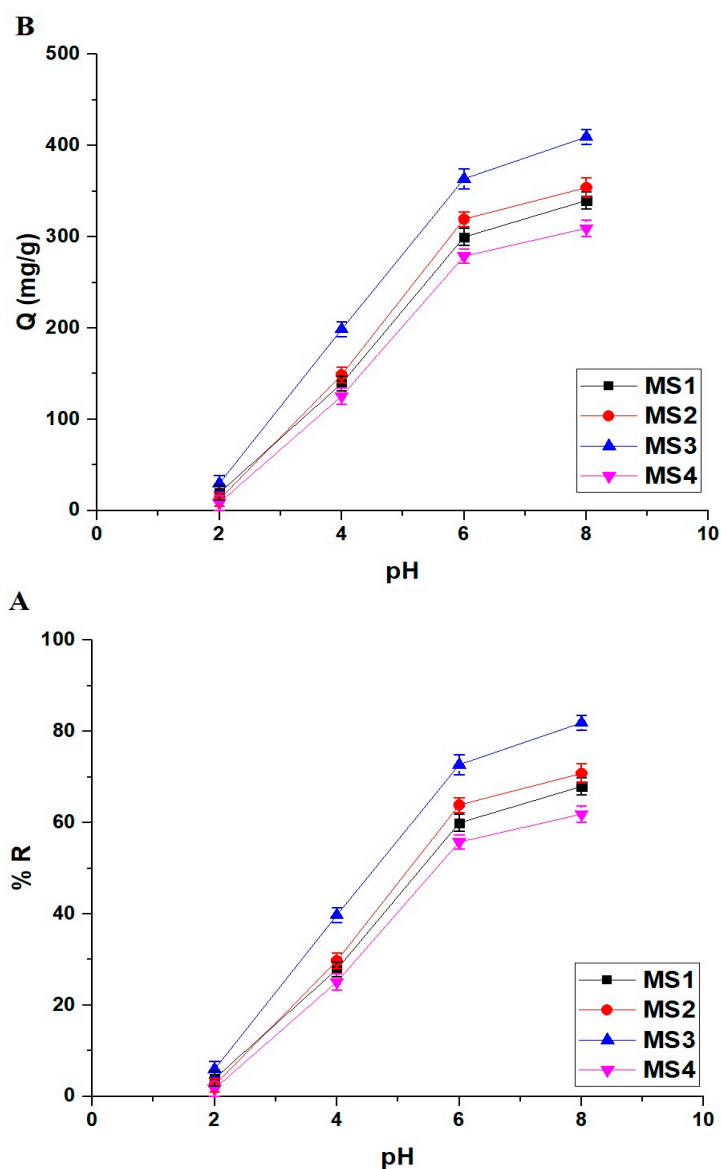


Figure 5. The FT-IR spectra of the MS1 (A), MS2 (B), MS3 (C), and MS4 (D) products.



**Figure 6.** Influence of initial pH of the crystal violet dye solution on the % disposal of the crystal violet dye (A) and the disposal capability of the MS1-MS4 adsorbents (B).

The point of zero charge (i.e.,  $\text{pH}_{\text{PZC}}$ ) of the MS1, MS2, MS3, and MS4 adsorbents is clarified in Figure 7. The  $\text{pH}_{\text{PZC}}$  of the MS1, MS2, MS3, and MS4 adsorbents is 5.30, 5.52, 5.62, and 5.69, respectively. In dye solutions whose pH value is smaller than  $\text{pH}_{\text{PZC}}$ ,  $\text{H}^+$  ions are easily available and compete with the cationic crystal violet dye to reach the surface of the adsorbent, which then decreases the amount of the crystal violet dye that can be adsorbed due to the repulsion. In dye solutions whose pH value is greater than  $\text{pH}_{\text{PZC}}$ ,  $\text{OH}^-$  ions are attracted to the adsorbent surface. The adsorbent's surface was dominated by a negative charge that can attract more positively charged crystal violet dye, as depicted in Scheme 1 [42]. After that, the  $\text{Na}^+$  ions of the adsorbent were ion-exchanged with cationic crystal violet dye. It is worth noting that the sodium ions in the adsorbent material arise to neutralize the negative charge of the nanostructures resulting from the chemical substitution of some divalent manganese ions for tetravalent silicon ions.

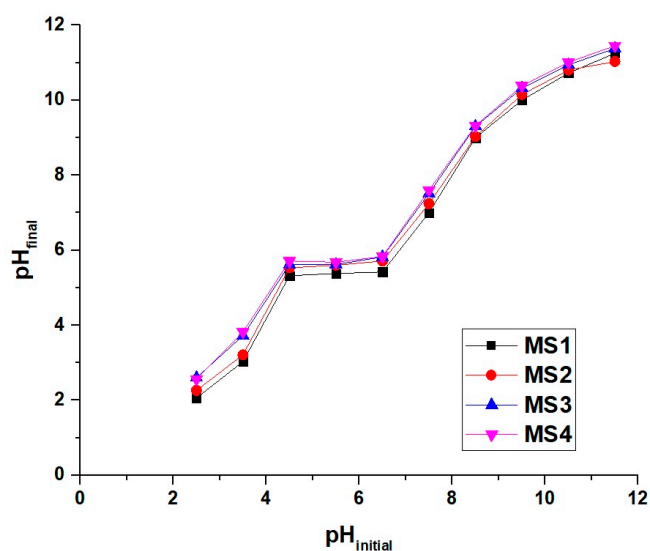
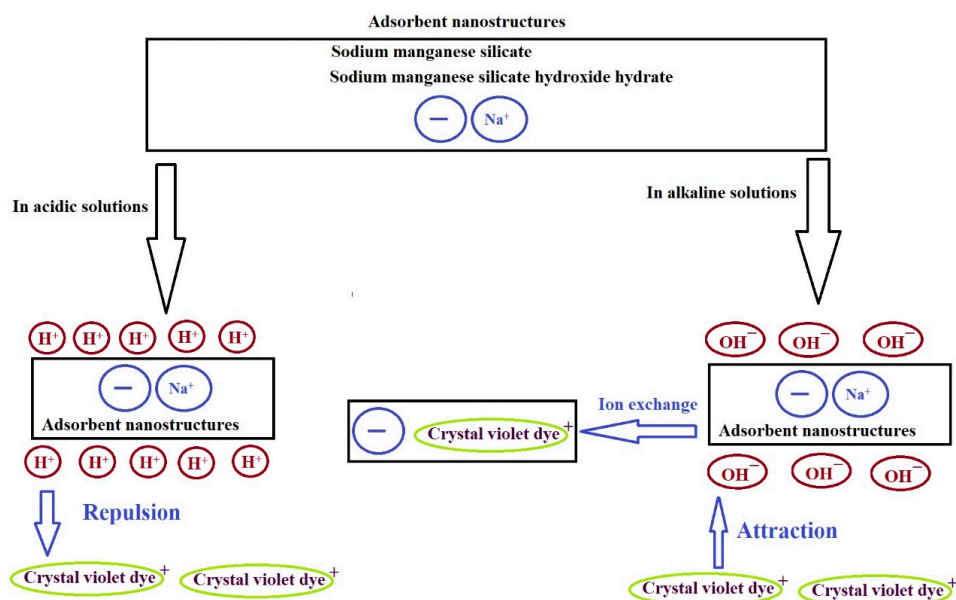
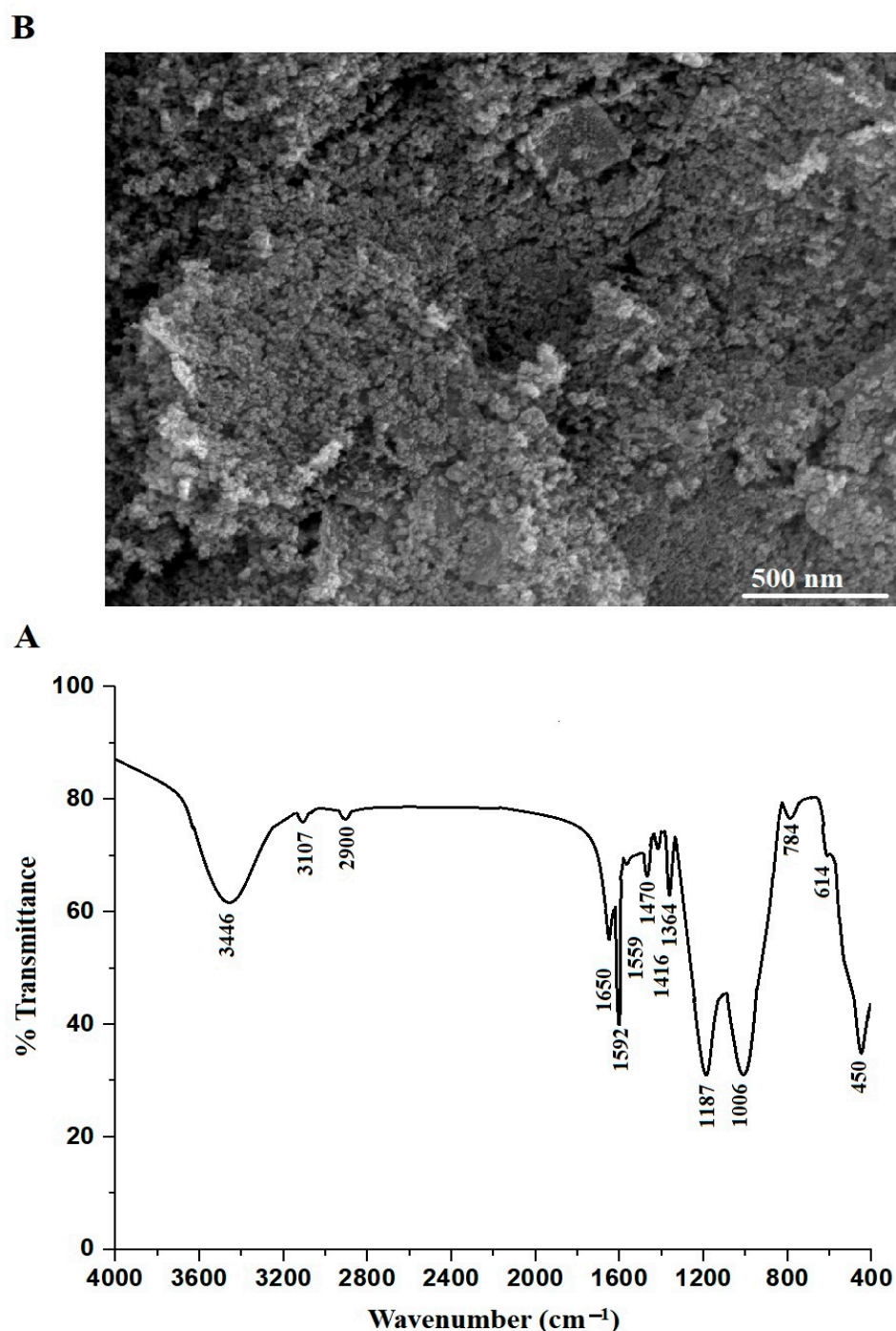


Figure 7. The point of zero charge of the MS1, MS2, MS3, and MS4 adsorbents.



Scheme 1. Schematic illustration of the crystal violet dye adsorption onto the MS1, MS2, MS3, and MS4 adsorbents under acidic and basic conditions.

To confirm the adsorption of crystal violet dye by the synthesized adsorbents, FT-IR analysis was performed for MS1 (as an illustrative example) after the adsorption of crystal violet dye, as shown in Figure 8A. The new bands at  $1187$  and  $1364\text{ cm}^{-1}$  are due to stretching vibrations of aliphatic and aromatic tertiary amine groups of crystal violet dye, respectively. Also, the new band at  $1470\text{ cm}^{-1}$  is due to the bending vibration of the  $\text{N-CH}_3$  group of crystal violet dye. Besides, the new band at  $1592\text{ cm}^{-1}$  is due to the stretching vibration of  $\text{C}=\text{C}$  aromatic of crystal violet dye. In addition, the new bands located at  $2900$  and  $3107\text{ cm}^{-1}$  are due to the stretching vibrations of aliphatic and aromatic  $\text{CH}$  of crystal violet dye, respectively [43]. The bands at  $450$ ,  $614$ ,  $784$ ,  $1006$ ,  $1416$ ,  $1559$ ,  $1650$ , and  $3446\text{ cm}^{-1}$  are due to the MS1 adsorbent. Besides, to confirm the adsorption of crystal violet dye by the synthesized adsorbents, SEM analysis was performed for MS1 (as an illustrative example) after the adsorption of crystal violet dye, as shown in Figure 8B. Figure 8B presents a clear visual depiction of the transformation in the morphology of the MS1 adsorbent, where the spherical and irregular shapes vanish as a result of the aggregation of crystal violet dye on its surface.



**Figure 8.** The FT-IR spectrum (A) and SEM image (B) of the MS1 sample after the adsorption of crystal violet dye.

### 3.2.2. Effect of Contact Time

The contact adsorption time has a major impact on the adsorption mechanism and performance. This study investigated the adsorption performance of the MS1, MS2, MS3, and MS4 adsorbents for crystal violet dye removal at different contact times, ranging from 20 min to 180 min, using an initial crystal violet dye concentration of 250 mg/L at room temperature and pH 8. Furthermore, the impact of contact adsorption time on the % disposal of crystal violet dye and the disposal capability of the MS1, MS2, MS3, and MS4 adsorbents is depicted in Figure 9A,B, respectively. It is evident that the % disposal of crystal violet dye and the disposal capability of the MS1, MS2, MS3, and MS4 adsorbents

were extremely sensitive to the contact time in the range from 20 min to 140 min because of the available active centers of adsorption. After that, the % disposal of crystal violet dye and the disposal capability of the MS1, MS2, MS3, and MS4 adsorbents were almost constant when the contact time of disposal increased from 140 min to 180 min because of the saturation of active centers of adsorption. After 140 min, the % disposal of the crystal violet dye using the MS1, MS2, MS3, and MS4 adsorbents is 67.56, 71.06, 81.41, and 61.44%, respectively. Besides, the maximum disposal capability of the MS1, MS2, MS3, and MS4 adsorbents towards crystal violet dye is 337.82, 355.28, 407.04, and 307.22 mg/g, respectively. A sudden increase in adsorption over a period of time (120–140 min) is due to the activation of adsorption sites. Adsorption typically occurs on the surface of the adsorbent material, which contains specific sites where adsorption can take place. If these adsorption sites are not immediately available for interaction with the adsorbate, the adsorption rate may initially be slow. However, with increasing time, these sites may become activated or exposed, leading to a sudden increase in adsorption.

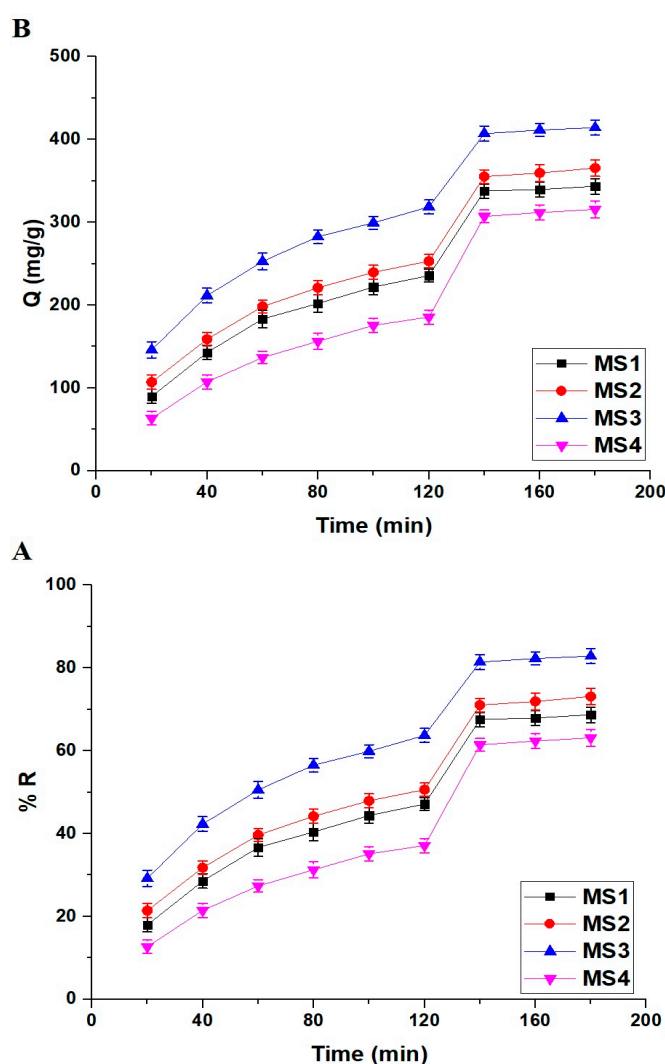


**Figure 9.** Effect of contact adsorption time on the % disposal of the crystal violet dye (A) and the disposal capability of the MS1-MS4 adsorbents (B).

Adsorption kinetics is a basic property for evaluating the effectiveness of an adsorption process. To describe the kinetics of the adsorption process, the linear forms of pseudo-2nd-order and pseudo-1st-order kinetic models have been utilized. The pseudo-1st-order model suggests that the rate of solute adsorption is directly proportional to the amount of adsorbate with time and difference between the saturation concentration. This kinetic

model is extremely appropriate during the starting step of the adsorption process. Using Equation (3), the linear form of the pseudo-1st-order equation is expressed [42].

$$\log(Q_e - Q_t) = \log Q_e - \frac{k_F}{2.303}t \quad (3)$$

where,  $Q_t$  represents the disposal capability of the MS1, MS2, MS3, or MS4 adsorbent at time  $t$  (mg/g),  $Q_e$  represents the quantity of the crystal violet dye adsorbed at the equilibrium (mg/g), and  $k_F$  represents the equilibrium rate constant of the pseudo-1st-order kinetic model (1/min). The pseudo-2nd-order kinetic model is based on the concept that chemical adsorption is the rate-limiting step. This kinetic model suggests that the adsorption rate is entirely dependent on the disposal capability and is independent of the adsorbate concentration. Using Equation (4), the linear form of the pseudo-2nd-order equation is expressed [42].

$$\frac{t}{Q_t} = \frac{1}{k_S Q_e^2} + \frac{1}{Q_e}t \quad (4)$$

where,  $k_S$  is the equilibrium rate constant of the pseudo-2nd-order kinetic model (g/mg.min). Figure 10A,B displays the pseudo-1st-order and pseudo-2nd-order linear kinetic models, respectively. Besides, Table 4 summarizes the corresponding kinetic constants.

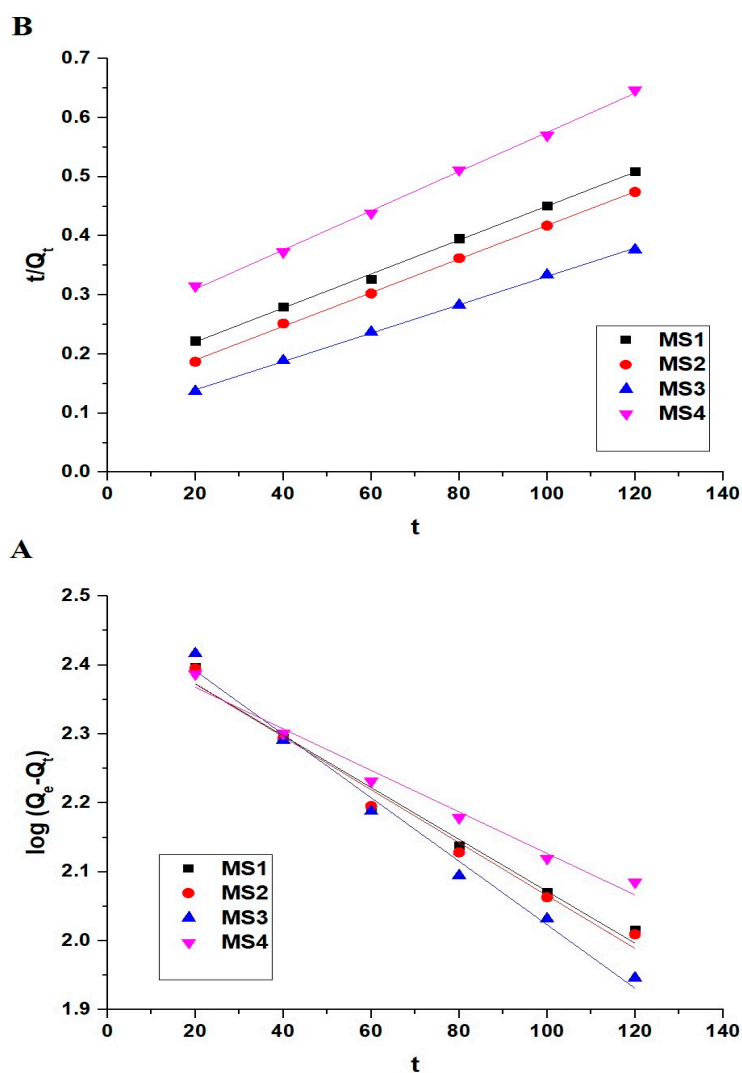


**Figure 10.** The linear pseudo-1st-order (A) and pseudo-2nd-order (B) models for the disposal of crystal violet dye using the MS1, MS2, MS3, and MS4 adsorbents.

**Table 4.** The kinetic constants of the linear pseudo-1st-order and pseudo-2nd-order models for the disposal of crystal violet dye using the MS1, MS2, MS3, and MS4 adsorbents.

Adsorbent	$Q_{Exp}$ (mg/g)	$Q_e$ (mg/g)		Rate Constants		$R^2$		RSS	
		First Order	Second Order	$k_F$ (1/min)	$k_S$ (g/mg.min)	First Order	Second Order	First Order	Second Order
MS1	337.82	280.56	348.43	0.0087	$5.05 \times 10^{-5}$	0.9763	0.9981	0.0019	$8.95 \times 10^{-5}$
MS2	355.28	281.27	350.88	0.0088	$6.10 \times 10^{-5}$	0.9799	0.9992	0.0017	$3.72 \times 10^{-5}$
MS3	407.04	304.53	416.67	0.0106	$6.29 \times 10^{-5}$	0.9849	0.9992	0.0018	$2.71 \times 10^{-5}$
MS4	307.22	267.77	302.11	0.0069	$4.49 \times 10^{-5}$	0.9782	0.9981	0.0011	$1.18 \times 10^{-4}$

Moreover, the nonlinear forms of pseudo-1st-order and pseudo-2nd-order kinetic models have been utilized as shown in Equations (5) and (6), respectively [1].

$$Q_t = Q_e (1 - e^{-k_F t}) \quad (5)$$

$$Q_t = \frac{Q_e^2 k_S t}{1 + Q_e k_S t} \quad (6)$$

Figure 11A,B shows the nonlinear pseudo-1st-order and pseudo-2nd-order kinetic models, respectively. Besides, Table 5 summarizes the corresponding kinetic constants. By comparing linear models with nonlinear ones, it can be concluded that nonlinear models are not suitable for describing adsorption processes because Reduced Chi-squared values ( $\chi^2$ ) are much larger than 1. Besides, linear models are suitable for describing adsorption processes because the values of the residual sum of squares (RSS) are very small. By comparing the linear pseudo-2nd-order model with the linear pseudo-1st-order model, it can be concluded that the linear pseudo-2nd-order model had the highest  $R^2$  (correlation co-efficient) values and the lowest RSS (residual sum of squares) values. Hence, the linear pseudo-2nd-order model better describes the disposal of the crystal violet dye using the MS1, MS2, MS3, and MS4 adsorbents than does the linear pseudo-1st-order. Also, the calculated theoretical disposal capability ( $Q_e$ ) values from the pseudo-2nd-order linear model closely matched with the experimental disposal capability ( $Q_{Exp}$ ) values.

### 3.2.3. Effect of Temperature

The temperature has a major impact on the adsorption mechanism and performance. This study investigated the adsorption performance of the MS1, MS2, MS3, and MS4 adsorbents for crystal violet dye removal at different temperatures, ranging from 298 kelvin to 328 kelvin, using an initial crystal violet dye concentration of 250 mg/L at pH 8 and 140 min. The effect of temperature on the % disposal of crystal violet dye and the disposal capability of the MS1, MS2, MS3, and MS4 adsorbents is depicted in Figure 12A,B, respectively. It is evident that the % disposal of crystal violet dye and the disposal capability of the MS1, MS2, MS3, and MS4 adsorbents were extremely decreased as the temperature increased. Higher temperatures can lead to desorption, where previously adsorbed molecules gain enough energy to break free from the surface. This process becomes more significant at higher temperatures, contributing to the decrease in adsorption.

The impact of temperature on the disposal of crystal violet dye using the MS1, MS2, MS3, and MS4 nanostructures was evaluated using the thermodynamic parameters, for example,  $\Delta G^\circ$  (change in free energy, kJ/mol),  $\Delta H^\circ$  (change in enthalpy, kJ/mol), and  $\Delta S^\circ$  (change in entropy, kJ/mol kelvin) which were evaluated using Equations Nos. (7)–(9) [42].

$$\ln K_d = \frac{\Delta S^\circ}{R} - \frac{\Delta H^\circ}{RT} \quad (7)$$

$$\Delta G^\circ = \Delta H^\circ - T \Delta S^\circ \quad (8)$$

$$K_d = \frac{Q_e}{C_e} \quad (9)$$

where,  $R$  represents the universal gas constant (kJ/mol kelvin),  $T$  represents the absolute temperature (kelvin), and  $K_d$  represents the distribution constant (L/g). The linear variation of  $\ln K_d$  against  $1/T$  is depicted in Figure 13, and the thermodynamic parameters can be calculated using intercept and slope. The examined thermodynamic parameters for the disposal of crystal violet dye by the MS1, MS2, MS3, and MS4 adsorbents are listed in Table 6. Negative  $\Delta G^\circ$  values revealed that the disposal of crystal violet dye using the MS1, MS2, MS3, and MS4 adsorbents is spontaneous. Besides, the negative  $\Delta H^\circ$  values revealed that the disposal of crystal violet dye using the MS1, MS2, MS3, and MS4 adsorbents is exothermic. Moreover, the positive  $\Delta S^\circ$  values indicated that the disposal of crystal violet dye using the MS1, MS2, MS3, and MS4 adsorbents was accomplished in the direction of increasing system randomness. Additionally, the disposal of the crystal violet dye using the MS1, MS2, MS3, and MS4 adsorbents is chemical in nature because the  $\Delta H^\circ$  values exceed 40 kJ/mol.

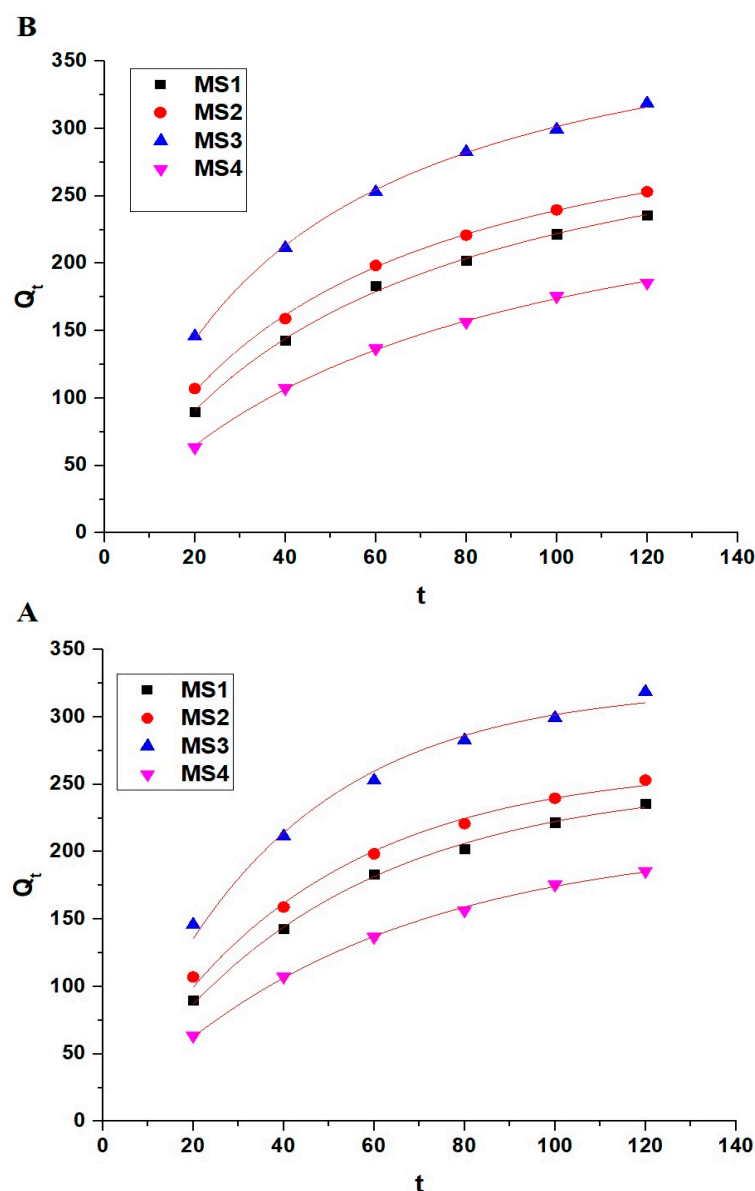


**Figure 11.** The nonlinear pseudo-1st-order (A) and pseudo-2nd-order (B) models for the disposal of crystal violet dye applying the MS1, MS2, MS3, and MS4 adsorbents.

**Table 5.** The kinetic constants of the nonlinear pseudo-1st-order and pseudo-2nd-order models for the disposal of crystal violet dye using the MS1, MS2, MS3, and MS4 adsorbents.

Adsorbent	$Q_{Exp}$ (mg/g)	$Q_e$ (mg/g)		Rate Constants		$R^2$		$\chi^2$	
		First Order	Second Order	$k_F$ (1/min)	$k_S$ (g/mg.min)	First Order	Second Order	First Order	Second Order
MS1	337.82	253.39	347.07	0.0210	$5.12 \times 10^{-5}$	0.9974	0.9983	9.54	6.35
MS2	355.28	264.63	351.87	0.0236	$6.04 \times 10^{-5}$	0.9936	0.9991	24.32	3.53
MS3	407.04	322.83	416.23	0.0272	$6.31 \times 10^{-5}$	0.9879	0.9988	62.19	6.28
MS4	307.22	210.45	299.66	0.0176	$4.61 \times 10^{-5}$	0.9989	0.9992	2.71	2.21

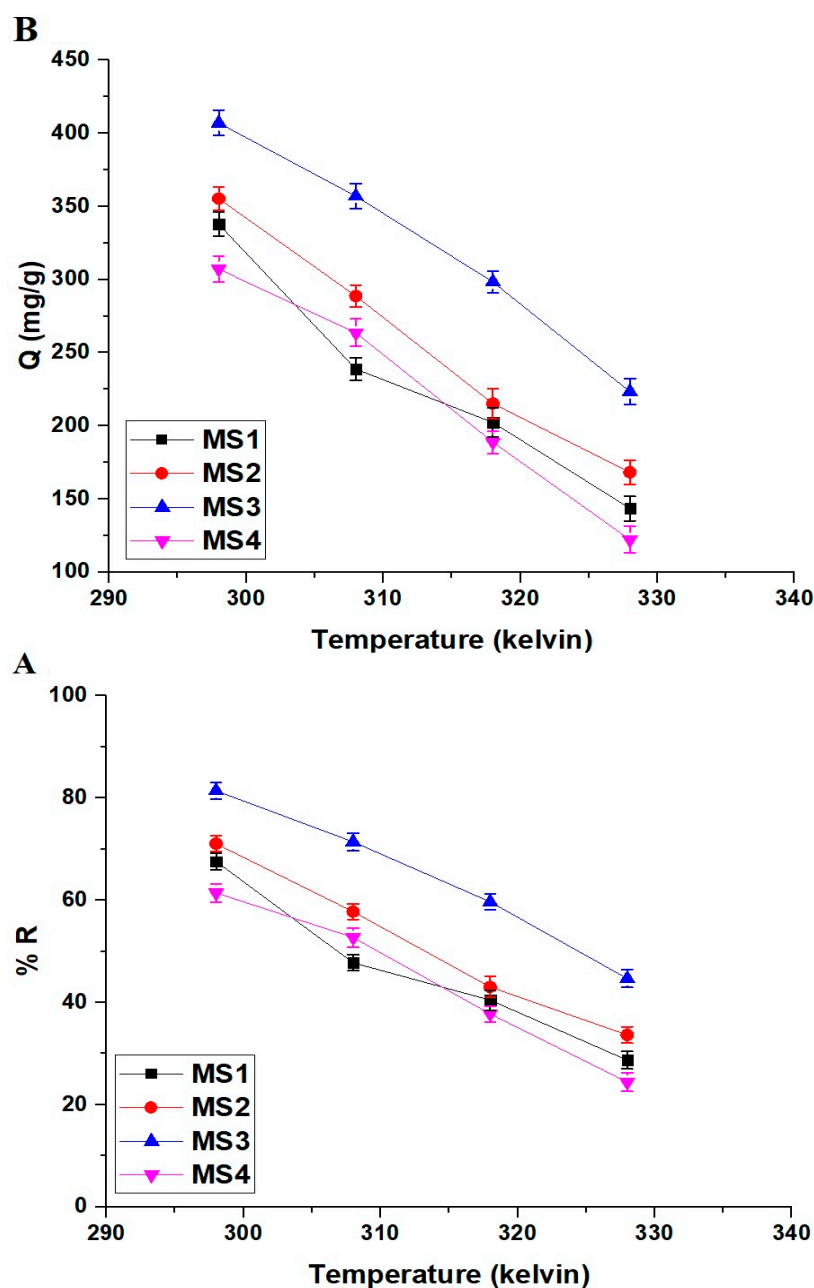


**Figure 12.** Effect of solution temperature on the % disposal of the crystal violet dye (A) and the disposal capability of the MS1-MS4 adsorbents (B).

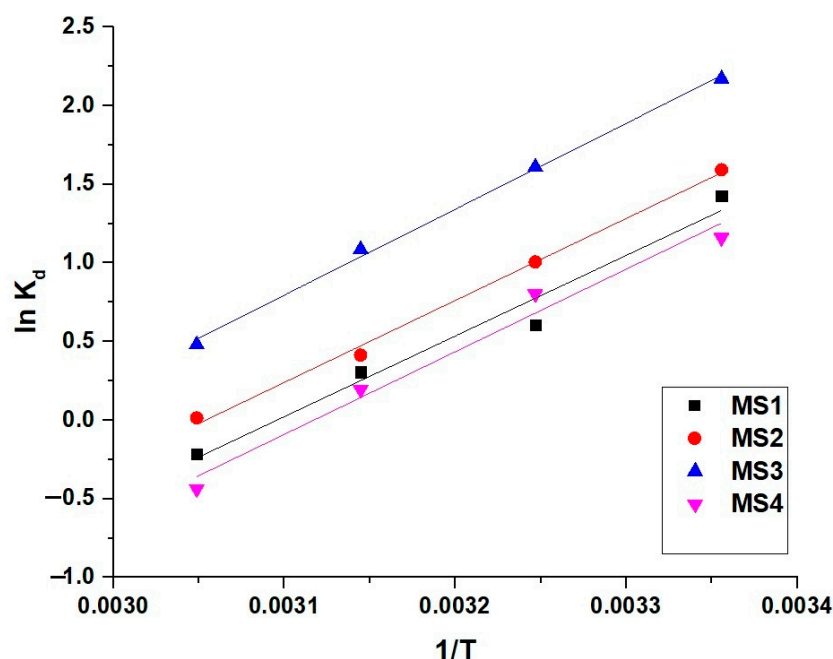


Figure 13. The linear variation of  $\ln K_d$  against  $1/T$ .

Table 6. The obtained thermodynamic parameters for the disposal of crystal violet dye utilizing the MS1, MS2, MS3, and MS4 adsorbents.

Adsorbent	$\Delta H^\circ$ (kJ/mol)	$\Delta S^\circ$ (kJ/mol Kelvin)	$\Delta G^\circ$ (kJ/mol)			
			298	308	318	328
MS1	−42.85	0.1326	−82.37	−83.69	−85.02	−86.35
MS2	−43.57	0.1331	−83.22	−84.55	−85.88	−87.21
MS3	−45.66	0.1349	−85.85	−87.20	−88.55	−89.90
MS4	−43.90	0.1368	−84.68	−86.05	−87.42	−88.79

### 3.2.4. Effect of Concentration

The concentration has a major impact on the adsorption mechanism and performance. This study investigated the adsorption performance of the MS1, MS2, MS3, and MS4 adsorbents for crystal violet dye removal at different concentrations, ranging from 150 mg/L to 300 mg/L at pH 8 and 140 min. The impact of initial dye concentration on the % disposal of crystal violet dye and the disposal capability of the MS1, MS2, MS3, and MS4 adsorbents is depicted in Figure 14A,B, respectively. It is evident that the % disposal of crystal violet dye using the MS1, MS2, MS3, and MS4 adsorbents was extremely decreased, whereas the disposal capability increased as the concentration increased. As the initial concentration of the contaminant increases, the absolute amount of contaminant being adsorbed also increases. However, the disposal percentage may decrease because the same amount of adsorption will result in a smaller relative reduction in the higher initial concentration.

The adsorption isotherm model illustrates the interaction between adsorbate and adsorbent, providing a theoretical foundation for the development of the dye adsorption mechanism. The maximum adsorption amount can be predicted using the linear Langmuir isotherm (Equation (10)), which assumes single molecular layer surface adsorption and uniform adsorption at each adsorption site [42].

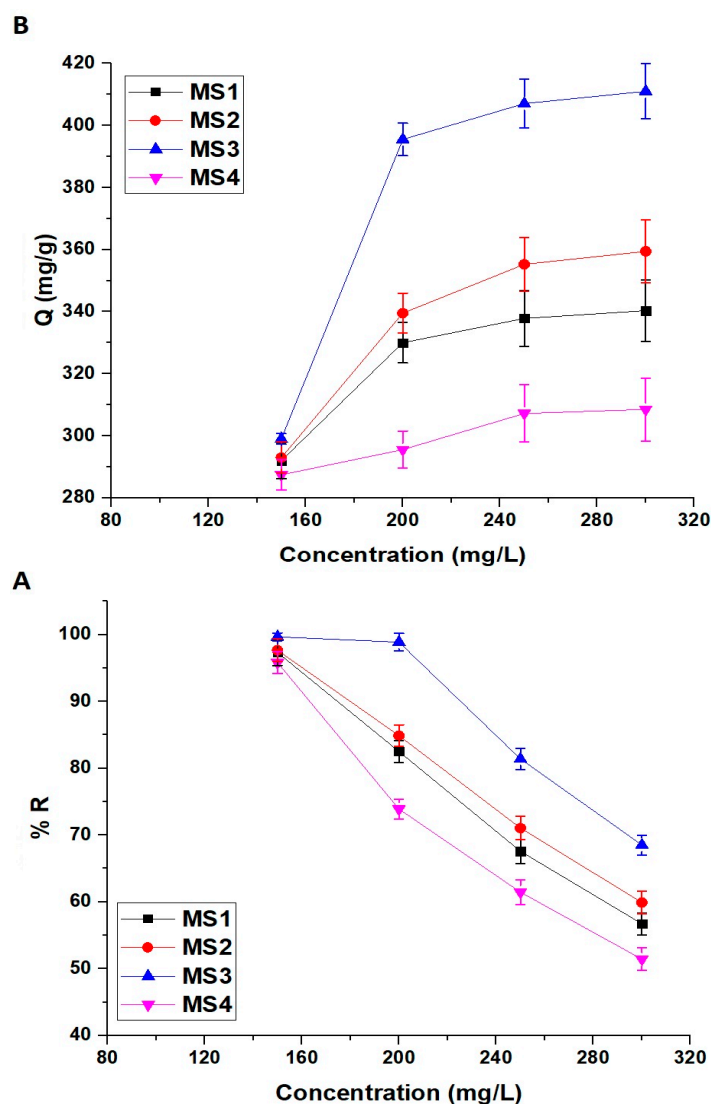


**Figure 14.** Effect of initial dye concentration on the % disposal of the crystal violet dye (A) and the disposal capability of the MS1-MS4 adsorbents (B).

$$\frac{C_e}{Q_e} = \frac{1}{k_L Q_{max}} + \frac{C_e}{Q_{max}} \quad (10)$$

where,  $k_L$  is the constant of Langmuir (L/mg) and  $Q_{max}$  is the maximum disposal capability of the MS1, MS2, MS3, and MS4 adsorbents (mg/g).

The linear Freundlich isotherm (Equation (11)) describes the adsorption of molecules on heterogeneous surfaces [42].

$$\ln Q_e = \ln k_{Fr} + \frac{1}{n} \ln C_e \quad (11)$$

where,  $k_{Fr}$  represents the constant of Freundlich ((mg/g) (L/mg) $^{1/n}$ ) whereas  $n$  is the strength factor of the adsorption process. The Freundlich isotherm can be applied to estimate the  $Q_{max}$  applying Equation (12) [42].

$$Q_{max} = k_{Fr} \left( C_o^{1/n} \right) \quad (12)$$

Figure 15A,B displays the linear Langmuir and Freundlich equilibrium isotherms, respectively. Besides, Table 7 summarizes the corresponding equilibrium constants.

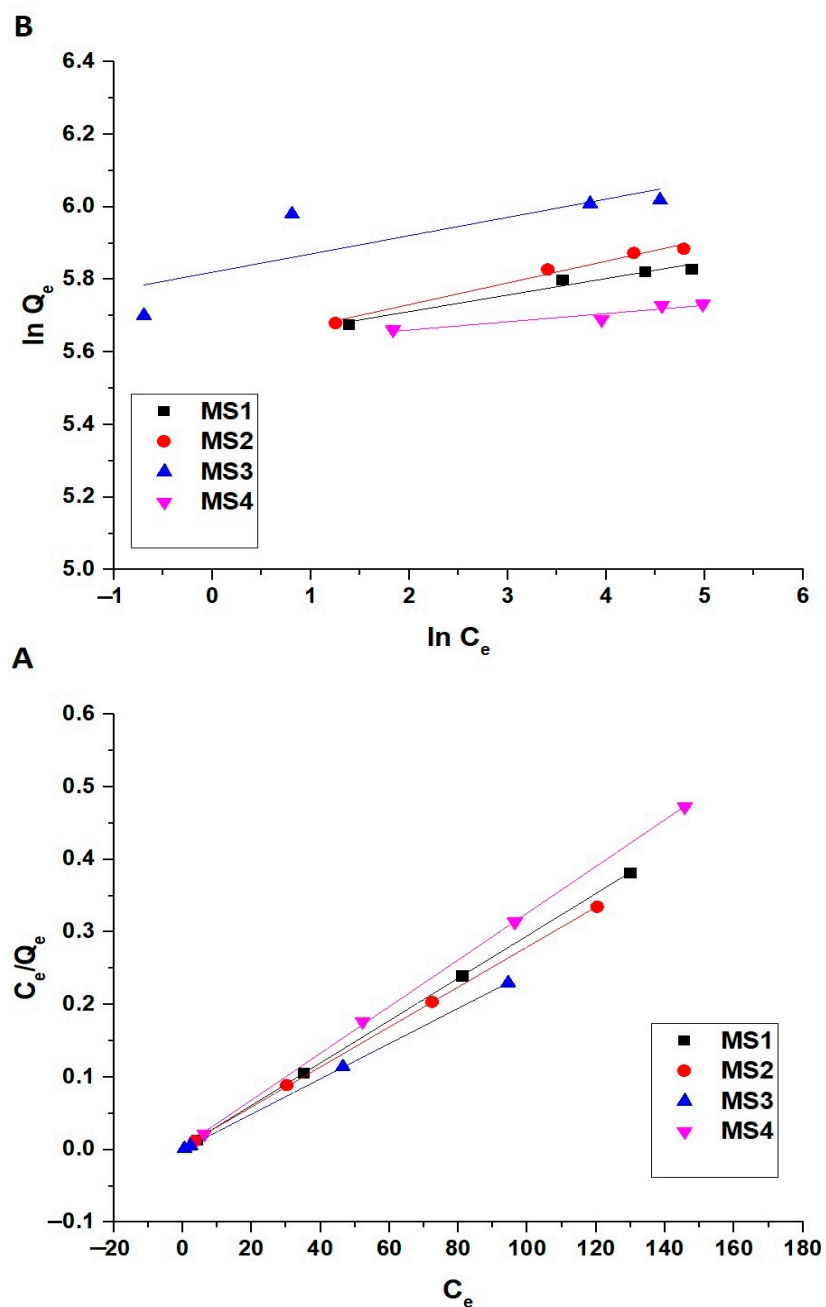


Figure 15. The linear Langmuir (A) and Freundlich (B) equilibrium isotherms for the disposal of crystal violet dye applying the MS1, MS2, MS3, and MS4 adsorbents.

Table 7. The constants of the linear Langmuir and Freundlich equilibrium isotherms for the adsorption of crystal violet dye applying the MS1, MS2, MS3, and MS4 adsorbents.

Adsorbent	Langmuir				Freundlich			
	$Q_{max}$ (mg/g)	$k_L$ (L/mg)	RSS	$R^2$	$Q_{max}$ (mg/g)	$k_{Fr}$ (mg/g)(L/mg) <sup>1/n</sup>	RSS	$R^2$
MS1	342.47	1.0069	$2.11 \times 10^{-6}$	0.9996	354.94	275.92	$7.77 \times 10^{-4}$	0.9533
MS2	362.32	0.7095	$6.53 \times 10^{-6}$	0.9998	380.34	273.46	$3.97 \times 10^{-4}$	0.9775
MS3	411.52	4.7178	$6.65 \times 10^{-7}$	0.9997	445.02	336.94	0.0224	0.5161
MS4	310.56	0.7541	$2.72 \times 10^{-5}$	0.9996	311.25	274.58	$3.62 \times 10^{-4}$	0.8394

Moreover, the nonlinear forms of Langmuir and Freundlich equilibrium isotherms have been utilized, as shown in Equations (13) and (14), respectively [1].

$$Q_e = \frac{Q_{max}k_L C_e}{1 + k_L C_e} \quad (13)$$

$$Q_e = k_{Fr} \times C_e^{1/n} \quad (14)$$

Figure 16A,B shows the nonlinear Langmuir and Freundlich equilibrium isotherms for the disposal of crystal violet dye onto the synthesized adsorbents, respectively. Besides, Table 8 summarizes the corresponding equilibrium constants.

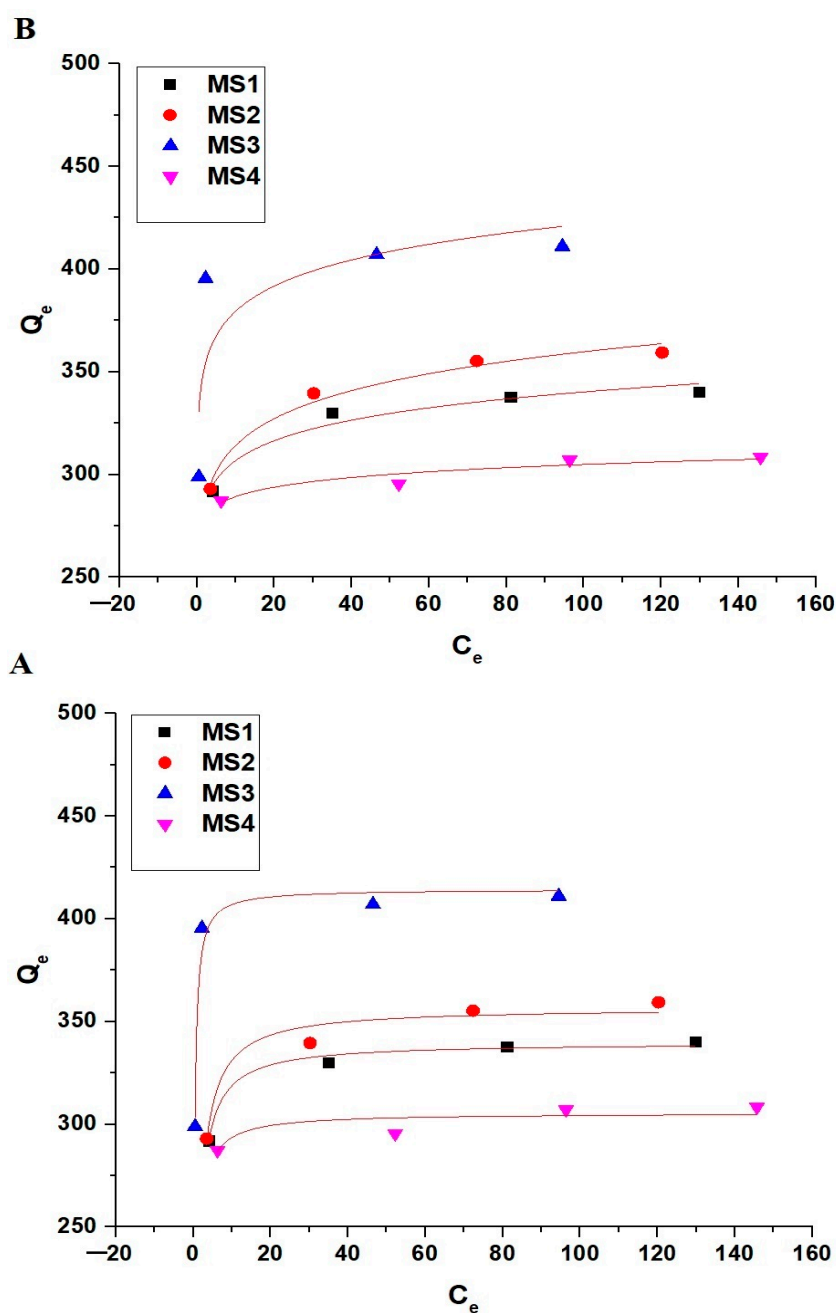


**Figure 16.** The nonlinear Langmuir (A) and Freundlich (B) equilibrium isotherms for the disposal of crystal violet dye applying the MS1, MS2, MS3, and MS4 adsorbents.

**Table 8.** The constants of the nonlinear Langmuir and Freundlich equilibrium isotherms for the adsorption of crystal violet dye applying the MS1, MS2, MS3, and MS4 adsorbents.

Adsorbent	Langmuir					Freundlich		
	$Q_{max}$ (mg/g)	$k_L$ (L/mg)	$R^2$	$\chi^2$	$1/n$	$k_{Fr}$ (mg/g) (L/mg) <sup>1/n</sup>	$R^2$	$\chi^2$
MS1	339.76	1.5149	0.9880	9.06	0.0449	276.61	0.9661	25.67
MS2	356.73	1.2894	0.9642	49.75	0.0589	274.26	0.9831	23.51
MS3	414.40	5.4610	0.9753	104.57	0.0461	341.23	0.6708	1395.98
MS4	305.47	2.4586	0.7295	40.73	0.0229	274.38	0.8922	16.23

By comparing linear isotherms with nonlinear ones, it can be concluded that non-linear isotherms are not suitable for describing adsorption processes because Reduced Chi-squared values ( $\chi^2$ ) are much larger than 1. Besides, linear isotherms are suitable for describing adsorption processes because the values of the residual sum of squares (RSS) are very small. By comparing the linear Langmuir isotherm with the linear Freundlich isotherm, it can be concluded that the linear Langmuir isotherm had the highest  $R^2$  (correlation co-efficient) values and the lowest RSS (residual sum of squares) values. Hence, the linear Langmuir isotherm better describes the disposal of the crystal violet dye using the MS1, MS2, MS3, and MS4 adsorbents than does the linear Freundlich isotherm. In addition, the maximum disposal capabilities of the MS1, MS2, MS3, and MS4 adsorbents towards crystal violet dye are 342.47, 362.32, 411.52, and 310.56 mg/g, respectively.

#### 4. Conclusions

Sodium manganese silicate/sodium manganese silicate hydroxide hydrate nanostructures were synthesized using the hydrothermal treatment of Mn(II)/Si(IV) gel at 180 °C for 6, 12, 18, and 24 h and abbreviated as MS1, MS2, MS3, and MS4, respectively. The synthesized nanostructures were successfully used to remove crystal violet dye from aquatic environments. The optimal crystal violet dye adsorption conditions were achieved at pH 8, 140 min, and 298 kelvin. In addition, the maximum disposal capabilities of the MS1, MS2, MS3, and MS4 adsorbents towards crystal violet dye are 342.47, 362.32, 411.52, and 310.56 mg/g, respectively.

**Author Contributions:** Conceptualization, E.A.A.; methodology, E.A.A. and G.S.E.-S.; formal analysis, E.A.A., G.S.E.-S. and H.S.A.; resources, E.A.A. and G.S.E.-S.; writing—original draft preparation, H.S.A., F.K.A. and M.S.B.; writing—review and editing, E.A.A., F.A.S., N.R. and K.u.R.; funding acquisition, H.S.A. All authors have read and agreed to the published version of the manuscript.

**Funding:** Princess Nourah bint Abdulrahman University Researchers Supporting Project number (PNURSP2023R185), Princess Nourah bint Abdulrahman University, Riyadh, Saudi Arabia.

**Data Availability Statement:** Not applicable.

**Conflicts of Interest:** The authors declare no conflict of interest.

#### References

- Ouachtak, H.; El Guerdaoui, A.; El Haouti, R.; Haounati, R.; Ighnih, H.; Toubi, Y.; Alakhras, F.; Rehman, R.; Hafid, N.; Addi, A.A.; et al. Combined Molecular Dynamics Simulations and Experimental Studies of the Removal of Cationic Dyes on the Eco-Friendly Adsorbent of Activated Carbon Decorated Montmorillonite Mt@AC. *RSC Adv.* **2023**, *13*, 5027–5044. [[CrossRef](#)]
- Song, J.; Chen, Y.; Luan, F. Air Pollution, Water Pollution and Robots: Is Technology the Panacea. *J. Environ. Manag.* **2023**, *330*, 117170. [[CrossRef](#)] [[PubMed](#)]
- Kausar, A.; Zohra, S.T.; Ijaz, S.; Iqbal, M.; Iqbal, J.; Bibi, I.; Nouren, S.; El Messaoudi, N.; Nazir, A. Cellulose-Based Materials and Their Adsorptive Removal Efficiency for Dyes: A Review. *Int. J. Biol. Macromol.* **2023**, *224*, 1337–1355. [[CrossRef](#)] [[PubMed](#)]
- Xiang, H.; Min, X.; Tang, C.J.; Sillanpää, M.; Zhao, F. Recent Advances in Membrane Filtration for Heavy Metal Removal from Wastewater: A Mini Review. *J. Water Process Eng.* **2022**, *49*, 103023. [[CrossRef](#)]

5. Ayalew, Z.M.; Guo, X.; Zhang, X. Synthesis and Application of Polyethyleneimine (PEI)-based Composite/Nanocomposite Material for Heavy Metals Removal from Wastewater: A Critical Review. *J. Hazard. Mater. Adv.* **2022**, *8*, 100158. [[CrossRef](#)]
6. Sankar Sana, S.; Haldhar, R.; Parameswaranpillai, J.; Chavali, M.; Kim, S.C. Silver Nanoparticles-Based Composite for Dye Removal: A Comprehensive Review. *Clean. Mater.* **2022**, *6*, 100161. [[CrossRef](#)]
7. Wang, J.; Sha, X.; Chen, X.; Zhuo, H.; Xie, W.; Zhou, Z.; He, X.; Wu, L.; Li, B. Removal and Distribution of Antibiotics and Resistance Genes in Conventional and Advanced Drinking Water Treatment Processes. *J. Water Process Eng.* **2022**, *50*, 103217. [[CrossRef](#)]
8. Pirsahab, M.; Moradi, N.; Hossini, H. Sonochemical Processes for Antibiotics Removal from Water and Wastewater: A Systematic Review. *Chem. Eng. Res. Des.* **2023**, *189*, 401–439. [[CrossRef](#)]
9. Jiang, Z.; Chen, M.; Lee, X.; Feng, Q.; Cheng, N.; Zhang, X.; Wang, S.; Wang, B. Enhanced Removal of Sulfonamide Antibiotics from Water by Phosphogypsum Modified Biochar Composite. *J. Environ. Sci.* **2023**, *130*, 174–186. [[CrossRef](#)]
10. Salahshoori, I.; Namayandeh, M.; Ghasemi, S.; Masoomeh, S.; Mirnezami, S.; Nobre, M.A.L.; Ali, H. Assessing Cationic Dye Adsorption Mechanisms on MIL-53 (Al) Nanostructured MOF Materials Using Quantum Chemical and Molecular Simulations: Toward Environmentally Sustainable Wastewater Treatment. *J. Water Process Eng.* **2023**, *55*, 104081. [[CrossRef](#)]
11. Lei, Y.; Zhao, J.; Song, H.; Yang, F.; Shen, L.; Zhu, L. Enhanced Adsorption of Dyes by Functionalized UiO-66 Nanoparticles: Adsorption Properties and Mechanisms. *J. Mol. Struct.* **2023**, *1292*, 136111. [[CrossRef](#)]
12. Zhang, S.; Pan, Y.; Wang, W.; Lin, R.; Liu, X. Carboxylated Cellulose-Based Aerogel with Cellular Pores Prepared by Stir Freezing for Cationic Dye Adsorption. *Process Saf. Environ. Prot.* **2023**, *177*, 807–817. [[CrossRef](#)]
13. Lu, H.; Yang, Q.; Huang, B.; Qi, J.; Wang, R.; Zhou, Q.; Chen, Q.; Zhu, L.; Jin, J.; Kong, Y. Removal Performance and Adsorption Kinetics of Dyes by a Co-Based Metal Organic Framework. *Microporous Mesoporous Mater.* **2023**, *360*, 112665. [[CrossRef](#)]
14. Abbou, B.; Lebki, I.; Ouaddari, H.; El, A.; Ezzahra, F.; Kadiri, L.; Ouass, A.; Lebki, A.; Housseine, E. Improved Removal of Methyl Orange Dye by Adsorption Using Modified Clay: Combined Experimental Study Using Surface Response Methodology. *Inorg. Chem. Commun.* **2023**, *155*, 111127. [[CrossRef](#)]
15. Thue, P.S.; Sophia, A.C.; Lima, E.C.; Wamba, A.G.N.; de Alencar, W.S.; dos Reis, G.S.; Rodembusch, F.S.; Dias, S.L.P. Synthesis and Characterization of a Novel Organic-Inorganic Hybrid Clay Adsorbent for the Removal of Acid Red 1 and Acid Green 25 from Aqueous Solutions. *J. Clean. Prod.* **2018**, *171*, 30–44. [[CrossRef](#)]
16. Li, Y.; Wang, S.; Shen, Z.; Li, X.; Zhou, Q.; Sun, Y.; Wang, T.; Liu, Y.; Gao, Q. Gradient Adsorption of Methylene Blue and Crystal Violet onto Compound Microporous Silica from Aqueous Medium. *ACS Omega* **2020**, *5*, 28382–28392. [[CrossRef](#)]
17. Hu, X.; Yan, L.; Wang, Y.; Xu, M. Freeze-Thaw as a Route to Build Manageable Polysaccharide Cryogel for Deep Cleaning of Crystal Violet. *Chem. Eng. J.* **2020**, *396*, 125354. [[CrossRef](#)]
18. Mittal, A.; Mittal, J.; Malviya, A.; Kaur, D.; Gupta, V.K. Adsorption of Hazardous Dye Crystal Violet from Wastewater by Waste Materials. *J. Colloid Interface Sci.* **2010**, *343*, 463–473. [[CrossRef](#)]
19. Mahmoud, M.E.; Nabil, G.M.; Khalifa, M.A.; El-Mallah, N.M.; Hassouba, H.M. Effective Removal of Crystal Violet and Methylene Blue Dyes from Water by Surface Functionalized Zirconium Silicate Nanocomposite. *J. Environ. Chem. Eng.* **2019**, *7*, 103009. [[CrossRef](#)]
20. Mahmood, O.A.A.Q.; Waisi, B.I. Crystal Violet Dye Removal from Aqueous Water Using Polyacrylonitrile Precursor Beads. *Mater. Today Proc.* **2021**, *42*, 2185–2192. [[CrossRef](#)]
21. Sanakousar, M.F.; Vidyasagar, C.C.; Jiménez-Pérez, V.M.; Jayanna, B.K.; Mounesh; Shridhar, A.H.; Prakash, K. Efficient Photocatalytic Degradation of Crystal Violet Dye and Electrochemical Performance of Modified MWCNTs/Cd-ZnO Nanoparticles with Quantum Chemical Calculations. *J. Hazard. Mater. Adv.* **2021**, *2*, 100004. [[CrossRef](#)]
22. Wasim, M.; Sabir, A.; Shafiq, M.; Khan, R.U. Mussel Inspired Surface Functionalization of Polyamide Membranes for the Removal and Adsorption of Crystal Violet Dye. *Dye. Pigment.* **2022**, *206*, 110606. [[CrossRef](#)]
23. Homagai, P.L.; Poudel, R.; Poudel, S.; Bhattarai, A. Adsorption and Removal of Crystal Violet Dye from Aqueous Solution by Modified Rice Husk. *Heliyon* **2022**, *8*, e09261. [[CrossRef](#)] [[PubMed](#)]
24. Muhiuddin, G.; Bibi, I.; Nazeer, Z.; Majid, F.; Kamal, S.; Kausar, A.; Raza, Q.; Alwadai, N.; Ezzine, S.; Iqbal, M. Synthesis of Ni Doped Barium Hexaferrite by Microemulsion Route to Enhance the Visible Light-Driven Photocatalytic Degradation of Crystal Violet Dye. *Ceram. Int.* **2023**, *49*, 4342–4355. [[CrossRef](#)]
25. Gad, Y.H.; Helal, R.H.; Radi, H.; El-nemr, K.F.; Khozemy, E.E. Preparation and Application of Irradiated Polyvinyl Alcohol/Starch/Pumice Composites for Adsorption of Basic Dye: Isotherm and Kinetics Study. *Int. J. Biol. Macromol.* **2023**, *249*, 126106. [[CrossRef](#)] [[PubMed](#)]
26. Türk, F.N.; Arslano, H. Use and Applications of Metal-Organic Frameworks (MOF) in Dye Adsorption: Review. *J. Environ. Chem. Eng.* **2023**, *11*, 110568. [[CrossRef](#)]
27. He, H.; Wen, J.; Zhao, Q.; Ke, G.; Yang, H. The Adsorption Activity and Mechanism of Common Tourmalines for Typical Anionic and Cationic Dyes. *Chem. Phys.* **2023**, *571*, 111938. [[CrossRef](#)]
28. Thakur, V.; Sharma, P.; Awasthi, A.; Guleria, A.; Singh, K. Utility of Acrylic Acid Grafted Lignocellulosic Waste Sugarcane Bagasse for the Comparative Study of Cationic and Anionic Dyes Adsorption Applications. *Environ. Nanotechnol. Monit. Manag.* **2023**, *20*, 100824. [[CrossRef](#)]
29. Wei, J.; Jia, J.; Liao, T. Highly Selective Adsorption of Dyes by Functional Hypercrosslinked-Polymers Prepared in a Facile and Chemically Stable Manner. *J. Environ. Chem. Eng.* **2023**, *11*, 110555. [[CrossRef](#)]

30. Shafiq, F.; Liu, C.; Zhou, H.; Chen, H.; Yu, S.; Qiao, W. Adsorption Mechanism and Synthesis of Adjustable Hollow Hydroxyapatite Spheres for Efficient Wastewater Cationic Dyes Adsorption. *Colloids Surf. A Physicochem. Eng. Asp.* **2023**, *672*, 131713. [[CrossRef](#)]
31. Sarabandan, M.; Bashiri, H.; Mousavi, S.M. Removal of Crystal Violet Dye by an Efficient and Low Cost Adsorbent: Modeling, Kinetic, Equilibrium and Thermodynamic Studies. *Korean J. Chem. Eng.* **2019**, *36*, 1575–1586. [[CrossRef](#)]
32. Jayasanthan Kumari, H.; Krishnamoorthy, P.; Arumugam, T.K.; Radhakrishnan, S.; Vasudevan, D. An Efficient Removal of Crystal Violet Dye from Waste Water by Adsorption onto TLAC/Chitosan Composite: A Novel Low Cost Adsorbent. *Int. J. Biol. Macromol.* **2017**, *96*, 324–333. [[CrossRef](#)] [[PubMed](#)]
33. Miyah, Y.; Lahrichi, A.; Idrissi, M.; Boujraf, S.; Taouda, H.; Zerrouq, F. Assessment of Adsorption Kinetics for Removal Potential of Crystal Violet Dye from Aqueous Solutions Using Moroccan Pyrophyllite. *J. Assoc. Arab Univ. Basic Appl. Sci.* **2017**, *23*, 20–28. [[CrossRef](#)]
34. Muthukumar, C.; Sivakumar, V.M.; Thirumarimurugan, M. Adsorption Isotherms and Kinetic Studies of Crystal Violet Dye Removal from Aqueous Solution Using Surfactant Modified Magnetic Nano-adsorbent. *J. Taiwan Inst. Chem. Eng.* **2016**, *63*, 354–362. [[CrossRef](#)]
35. Sabna, V.; Thampi, S.G.; Chandrakaran, S. Adsorption of Crystal Violet onto Functionalised Multi-Walled Carbon Nanotubes: Equilibrium and Kinetic Studies. *Ecotoxicol. Environ. Saf.* **2016**, *134*, 390–397. [[CrossRef](#)]
36. Loganathan, M.; Raj, A.S.; Murugesan, A.; Kumar, P.S. Effective Adsorption of Crystal Violet onto Aromatic Polyimides: Kinetics and Isotherm Studies. *Chemosphere* **2022**, *304*, 135332. [[CrossRef](#)] [[PubMed](#)]
37. Foroutan, R.; Peighambaroust, S.J.; Peighambaroust, S.H.; Pateiro, M.; Lorenzo, J.M. Adsorption of Crystal Violet Dye Using Activated Carbon of Lemon Wood and Activated Carbon/Fe<sub>3</sub>O<sub>4</sub> Magnetic Nanocomposite from Aqueous Solutions: A Kinetic, Equilibrium and Thermodynamic Study. *Molecules* **2021**, *26*, 2241. [[CrossRef](#)]
38. Poudel, M.B.; Kim, H.J. Synthesis of High-Performance Nickel Hydroxide Nanosheets/Gadolinium Doped- $\alpha$ -MnO<sub>2</sub> Composite Nanorods as Cathode and Fe<sub>3</sub>O<sub>4</sub>/GO Nanospheres as Anode for an All-Solid-State Asymmetric Supercapacitor. *J. Energy Chem.* **2021**, *64*, 475–484. [[CrossRef](#)]
39. Yang, B.; Zhou, X.; Chen, Y.; Fang, Y.; Luo, H. Preparation of a Spindle  $\delta$ -MnO<sub>2</sub>@Fe/Co-MOF-74 for Effective Adsorption of Arsenic from Water. *Colloids Surf. A Physicochem. Eng. Asp.* **2021**, *629*, 127378. [[CrossRef](#)]
40. Khalifa, M.E.; Abdelrahman, E.A.; Hassanien, M.M.; Ibrahim, W.A. Application of Mesoporous Silica Nanoparticles Modified with Dibenzoylmethane as a Novel Composite for Efficient Removal of Cd(II), Hg(II), and Cu(II) Ions from Aqueous Media. *J. Inorg. Organomet. Polym. Mater.* **2020**, *30*, 2182–2196. [[CrossRef](#)]
41. Abdelrahman, E.A.; Hegazey, R.M.; El-Azabawy, R.E. Efficient Removal of Methylene Blue Dye from Aqueous Media Using Fe/Si, Cr/Si, Ni/Si, and Zn/Si Amorphous Novel Adsorbents. *J. Mater. Res. Technol.* **2019**, *8*, 5301–5313. [[CrossRef](#)]
42. Al-Wasidi, A.S.; Naglah, A.M.; Saad, F.A.; Abdelrahman, E.A. Modification of Silica Nanoparticles with 1-Hydroxy-2-Acetonaphthone as a Novel Composite for the Efficient Removal of Ni(II), Cu(II), Zn(II), and Hg(II) Ions from Aqueous Media. *Arab. J. Chem.* **2022**, *15*, 104010. [[CrossRef](#)]
43. Cheriaa, J.; Khairiddine, M.; Rouabhia, M.; Bakhrouf, A. Removal of Triphenylmethane Dyes by Bacterial Consortium. *Sci. World J.* **2012**, *2012*, 1–9. [[CrossRef](#)] [[PubMed](#)]

**Disclaimer/Publisher's Note:** The statements, opinions and data contained in all publications are solely those of the individual author(s) and contributor(s) and not of MDPI and/or the editor(s). MDPI and/or the editor(s) disclaim responsibility for any injury to people or property resulting from any ideas, methods, instructions or products referred to in the content.